Proceeding of the 2004 American Control Conference
Boston, Massachusetts June 30 - July 2, 2004

Unstable modes versus non-normal modes in supercritical channel flows

Mihailo R. Jovanović
jmihailo@engr.ucsb.edu

Bassam Bamieh
bamieh@engr.ucsb.edu

Department of Mechanical & Environmental Engineering
University of California, Santa Barbara, CA 93106-5070

Abstract— **We propose a measure to quantify the relative importance of unstable and non-normal modes in supercritical channel flows. The effect of non-normal modes is quantified by measuring the response of the flow to body force excitations. In the supercritical regime, unstable modes in channel flows grow relatively slowly, and we show that when compared over long but finite times, non-normal modes dominate the dynamics by orders of magnitude. Our analysis method is based on computing so-called exponentially discounted input-output system gains. It is well known that non-normal modes in the form of elongated streamwise structures prevail over Tollmien-Schlichting (TS) modes in subcritical channel flows. Our method of analysis shows that effectively, this is also the situation in the supercritical regime.**

Index Terms— **Supercritical Channel Flows; Non-normal Modes; Input-output System Gains.**

I. Introduction

It has become clear from recent work (see the recent monograph [1], and references therein for extensive review) that the so-called non-normal modes in the form of elongated streamwise structures dominate TS waves in subcritical channel flows. This can be established by a variety of methods that quantify the energy of flow perturbations rather than simply their asymptotic behavior as is done in traditional linear hydrodynamic stability [2]. For example, despite the fact that the equations represent a stable evolution (for e.g. Hagen-Poiseuille and Couette flows, or Poiseuille flow for Reynolds numbers below 5772), when measured in terms of the pseudo-spectrum (which quantifies the possibility of instability when perturbations in the dynamical equations are present) the so-called margin of stability is very small, and decreases with Reynolds number [3]–[7]. Another method of analysis involves the construction of initial flow configurations where the energy of the subsequent subcritical flow experiences large transient growth followed by a very slow eventual decay [8]–[10]. Yet a third method of analysis involves the introduction of body force fields as external excitations, which are arguably present in all physical flow problems. One then studies the so-called 'input-output resonances' of the resulting equations, and discovers that they occur at very different spatio-temporal frequencies than the poorly damped modes of the system [11]–[15]. These poorly damped modes represent the TS waves, while the input-output resonances are related to the streamwise vortices and streaks, which are ubiquitous in transitioning shear flows and fully turbulent boundary layers.

All of the above analysis methods discussed are applicable only to subcritical (i.e., linearly stable) flows. In this paper, we show that at least the input-output method can be generalized to supercritical flows by considering either finite time evolution or by measuring the size of perturbations with appropriate exponential discounts on their energies. Since the unstable modes of these equations in, for example, Poiseuille flow have very slow growth rates, it is relevant to investigate whether dominant supercritical flow structures on finite time intervals correspond to the structures generated by these exponentially growing modes or by something else. We illustrate how input-output system norms can be computed for supercritical fluid flows and show that even a small amount of noise in these flows yields completely different flow patterns from the ones corresponding to the exponentially growing system modes when finite time phenomena are considered. In particular, our results underscore the importance of the streamwise elongated flow structures (that is, streamwise vortices and streaks) not only in the subcritical channel flows, but also in the channel flows taking place in the supercritical regimes.

Our presentation is organized as follows: in section II, we briefly describe the externally excited Linearized Navier-Stokes (LNS) equations. In § III, we give a background material on the available tools for the input-output analysis of the LNS equations in channel flows. In § III-A and § III-B, we define the notions of finite horizon and exponentially discounted system norms, respectively. In § IV, we study the input-output gains in subcritical Poiseuille flow with $R = 5700$, and the exponentially discounted input-output gains in supercritical Poiseuille flow with $R = 10000$. We end our presentation with some concluding remarks in § V.

II. Dynamical description of flow fluctuations

We consider incompressible externally excited LNS equations in channel flow geometry shown in Figure 1. Using incompressibility condition pressure can be eliminated from the LNS which results in the so-called 'wall-normal velocity-vorticity' formulation of these equations [1]. After application of Fourier transform in the translation invariant (streamwise and spanwise) directions this representation, together with an equation for the velocity field components, can be expressed as [14]–[16]

$$\begin{aligned} \partial_t \psi(k_x, y, k_z, t) &= [\mathcal{A}(k_x, k_z)\psi(k_x, k_z, t)](y) + \\ &\quad [\mathcal{B}(k_x, k_z)\mathbf{d}(k_x, k_z, t)](y), \qquad (1) \\ \phi(k_x, y, k_z, t) &= [\mathcal{C}(k_x, k_z)\psi(k_x, k_z, t)](y), \end{aligned}$$

where k_x and k_z represent the streamwise and the spanwise wave-numbers, whereas the vector valued fields ψ, $\mathbf{d}$, and ϕ are respectively defined by $\psi := \begin{bmatrix} v & \omega_y \end{bmatrix}^T$, $\mathbf{d} := \begin{bmatrix} d_x & d_y & d_z \end{bmatrix}^T$, and $\phi := \begin{bmatrix} u & v & w \end{bmatrix}^T$. Note that we use the same symbol to denote a field and its Fourier transform. The reason for writing the equations in the above form is to regard the vector field ψ as the 'state' of the system (from which any other field can be computed at a given point in time), $\mathbf{d}$ as an input, and ϕ as an output. This is the so-called *state-space* form of driven dynamical systems common in the Dynamics and Controls literature [17]. State of

0-7803-8335-4/04/$17.00 ©2004 AACC

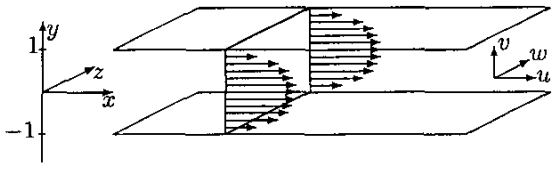

Fig. 1. Three dimensional Poiseuille flow.

the system is expressed in terms of the wall-normal velocity v and vorticity ω_y fields, the streamwise and the spanwise velocity components are denoted by u and w, whereas d_x, d_y, and d_z represent components of the forcing field $\mathbf{d}$ in x, y, and z directions, respectively. We remark that $\mathcal{A}$, $\mathcal{B}$, and $\mathcal{C}$ represent one-dimensional operators in the wall-normal direction which are, for a nominal velocity profile of the form $\begin{bmatrix} U(y) & 0 & 0 \end{bmatrix}^T$, given by

$$\mathcal{A} := \begin{bmatrix} \mathcal{A}_{11} & 0 \\ \mathcal{A}_{21} & \mathcal{A}_{22} \end{bmatrix}, \quad \mathcal{B} := \begin{bmatrix} \mathcal{B}_x & \mathcal{B}_y & \mathcal{B}_z \end{bmatrix},$$

$$\mathcal{A}_{11} := -\mathrm{i}k_x\Delta^{-1}U\Delta + \mathrm{i}k_x\Delta^{-1}U'' + \frac{1}{R}\Delta^{-1}\Delta^2,$$

$$\mathcal{A}_{22} := -\mathrm{i}k_xU + \frac{1}{R}\Delta,$$

$$\mathcal{A}_{21} := -\mathrm{i}k_zU',$$

$$\mathcal{B}_x := \begin{bmatrix} -\mathrm{i}k_x\Delta^{-1}\partial_y \\ \mathrm{i}k_z \end{bmatrix}, \quad \mathcal{B}_y := \begin{bmatrix} -(k_x^2+k_z^2)\Delta^{-1} \\ 0 \end{bmatrix},$$

$$\mathcal{B}_z := \begin{bmatrix} -\mathrm{i}k_z\Delta^{-1}\partial_y \\ -\mathrm{i}k_x \end{bmatrix},$$

$$\mathcal{C} := \begin{bmatrix} \mathcal{C}_u \\ \mathcal{C}_v \\ \mathcal{C}_w \end{bmatrix} := \frac{1}{k_x^2+k_z^2}\begin{bmatrix} \mathrm{i}k_x\partial_y & -\mathrm{i}k_z \\ k_x^2+k_z^2 & 0 \\ \mathrm{i}k_z\partial_y & \mathrm{i}k_x \end{bmatrix},$$

where i is the imaginary unit, R is the Reynolds number, $U' := \mathrm{d}U(y)/\mathrm{d}y$, and $\Delta := \partial_{yy} - k_x^2 - k_z^2$. The boundary conditions on v and ω_y are derived from the original no-slip boundary conditions and can be written as: $v(k_x, \pm 1, k_z, t) = \partial_y v(k_x, \pm 1, k_z, t) = \omega_y(k_x, \pm 1, k_z, t) = 0$, $\forall\ k_x, k_z \in \mathbb{R}$, $\forall\ t \geq 0$. The initial conditions on these fields are assumed to be identically equal to zero, that is $v(k_x, y, k_z, 0) = \omega_y(k_x, y, k_z, 0) = 0$, $\forall\, k_x, k_z \in \mathbb{R}$, $\forall\, y \in [-1, 1]$.

In § III, we give a background material on the available tools for the input-output analysis of the LNS equations in channel flows, and introduce the notions of finite horizon and exponentially discounted system norms.

III. Input-Output System Gains

There are two main tools in the input-output analysis of linear spatially-distributed dynamical systems. These are the spatio-temporal frequency and impulse responses respectively, and they will be precisely defined in the sequel. Given a particular frequency response, there is a unique corresponding impulse response that can be derived from it.

The *spatio-temporal frequency response* of system (1) is given by

$$\mathcal{H}(k_x, k_z, \omega) = \mathcal{C}(k_x, k_z)(\mathrm{i}\omega I - \mathcal{A}(k_x, k_z))^{-1}\mathcal{B}(k_x, k_z), \tag{2}$$

where ω denotes the temporal frequency. The frequency response is obtained directly from the Fourier symbols of the operators defining the state-space realization. The *spatio-temporal impulse response* of system (1) is determined by

$$\mathcal{H}(k_x, k_z, t) = \mathcal{C}(k_x, k_z)\mathrm{e}^{\mathcal{A}(k_x,k_z)t}\mathcal{B}(k_x, k_z), \tag{3}$$

where $\mathrm{e}^{\mathcal{A}t}$ denotes the symbol for the operator semigroup generated by $\mathcal{A}$ [17]. Clearly, (3) represents an inverse temporal Fourier transform of (2). Both these responses represent operators that map input fields into the appropriate output fields.

The frequency response of a system with a stable generator $\mathcal{A}$ has two interesting physical interpretations:

- it describes how the system responds to persistent (i.e., applied since $t = -\infty$) harmonic input signals,
- it describes the steady-state response to harmonic input signals applied over the time interval $0 \leq t < \infty$.

Namely, if the input is 'harmonic' in x, z, and t, i.e. $\mathbf{d}(x, y, z, t) = \bar{\mathbf{d}}(y)\mathrm{e}^{\mathrm{i}(\bar{k}_x x + \bar{k}_z z + \bar{\omega} t)}$, with $\bar{\mathbf{d}}(y)$ being some spatial distribution in the wall-normal direction, then the output is also harmonic in these directions of the same frequencies but with a modified amplitude and phase

$$\begin{aligned} \phi(x, y, z, t) &= \left[\mathcal{H}(\bar{k}_x, \bar{k}_z, \bar{\omega})\bar{\mathbf{d}}\right](y)\mathrm{e}^{\mathrm{i}(\bar{k}_x x + \bar{k}_z z + \bar{\omega} t)} \\ &= \int_{-1}^{1} \left[\mathcal{H}(\bar{k}_x, \bar{k}_z, \bar{\omega})\right](y, \eta)\bar{\mathbf{d}}(\eta)\,\mathrm{d}\eta \times \\ &\quad \mathrm{e}^{\mathrm{i}(\bar{k}_x x + \bar{k}_z z + \bar{\omega} t)}, \end{aligned} \tag{4}$$

where the amplitude and phase gain is precisely determined by $\mathcal{H}(\bar{k}_x, \bar{k}_z, \bar{\omega})$: the value of the frequency response at the input frequencies $(\bar{k}_x, \bar{k}_z, \bar{\omega})$. With a slight abuse of notation we use the same notation in (4) for the frequency response operator $\mathcal{H}(\bar{k}_x, \bar{k}_z, \bar{\omega})$ and its kernel representation $\left[\mathcal{H}(\bar{k}_x, \bar{k}_z, \bar{\omega})\right](y, \eta)$. The time interval on which a harmonic input is applied determines whether the output of a stable system is precisely given by (4) or whether it asymptotically converges to it.

On the other hand, the terminology for the spatio-temporal impulse response is due the fact that the kernel representation $[\mathcal{H}(k_x, k_z, t)](y, y_0)$ of operator $\mathcal{H}(k_x, k_z, t)$ represents the solution of system (1) to a spatio-temporal impulsive input function of the form $\delta(y - y_0, t)$. The response to any other forcing field $\mathbf{d}(k_x, y, k_z, t)$ is then obtained as the superposition of a spatially and temporally shifted family of impulse responses

$$\begin{aligned} &\phi(k_x, y, k_z, t) = \\ &\int_{-1}^{1}\int_{0}^{\infty} \left[\mathcal{H}(k_x, k_z, t-\tau)\right](y, \eta)\ \mathbf{d}(k_x, \eta, k_z, \tau)\,\mathrm{d}\tau\,\mathrm{d}\eta. \end{aligned} \tag{5}$$

Since $\mathcal{H}$ is a function of three independent variables there is a variety of different ways to visualize system properties. For example, one can study the maximal singular values of the operator $\mathcal{H}$

$$\sigma_{\max}^2(\mathcal{H}(k_x, k_z, \omega)) := \lambda_{\max}\{\mathcal{H}^*(k_x, k_z, \omega)\mathcal{H}(k_x, k_z, \omega)\},$$

or compute the Hilbert–Schmidt norm of $\mathcal{H}$

$$\|\mathcal{H}(k_x, k_z, \omega)\|_{HS}^2 := \mathrm{trace}(\mathcal{H}^*(k_x, k_z, \omega)\mathcal{H}(k_x, k_z, \omega)),$$

where $\mathcal{H}^*$ represents adjoint of operator $\mathcal{H}$. For any triple (k_x, k_z, ω), $\sigma_{\max}(\mathcal{H}(k_x, k_z, \omega))$ determines the largest 'amplification' from $\mathbf{d}$ to ϕ, with maximization being performed over wall-normal shapes. On the other hand, the Hilbert–Schmidt norm of $\mathcal{H}$ quantifies the Power Spectral Density of the output field in the presence of harmonic (in x and z) white, unit variance, temporally stationary stochastic (in y and t) external excitations. Furthermore, suprema or averages over different frequencies can be determined as well, e.g. by computing the temporal-supremum of the maximal singular values of the operator $\mathcal{H}$

$$[\|\mathcal{H}\|_\infty](k_x, k_z) := \sup_{\omega} \sigma_{\max}(\mathcal{H}(k_x, k_z, \omega)), \tag{6}$$

or the temporal-average of the Hilbert–Schmidt norm of the operator $\mathcal{H}$

$$\begin{aligned}\left[\|\mathcal{H}\|_2^2\right](k_x,k_z) &:= \frac{1}{2\pi}\int_{-\infty}^{\infty}\|\mathcal{H}(k_x,k_z,\omega)\|_{HS}^2\,\mathrm{d}\omega \\ &= \int_0^{\infty}\|\mathcal{H}(k_x,k_z,t)\|_{HS}^2\,\mathrm{d}t.\end{aligned} \tag{7}$$

Notation used in (6) and (7) indicates that the corresponding quantities represent, for any given pair (k_x,k_z), $\mathcal{H}_\infty$ and $\mathcal{H}_2$–norms of system (1) [18], respectively. We remark that both these norms have interesting physical interpretations. Namely, for any given pair (k_x,k_z), the $\mathcal{H}_\infty$–norm represents the worst case amplification of purely harmonic (in x and z) deterministic (in y and t) disturbances. This worst case input-output gain is obtained by maximizing over input temporal frequencies and wall-normal shapes. This quantity also has an interesting time domain interpretation. It is a standard fact from linear systems theory [18] that the $\mathcal{H}_\infty$–norm represents the induced 2–norm in the temporal domain

$$\left[\|\mathcal{H}\|_\infty\right](k_x,k_z) = \sup_{[\|\mathbf{d}\|_2](k_x,k_z)\,\leq\,1}\frac{[\|\phi\|_2](k_x,k_z)}{[\|\mathbf{d}\|_2](k_x,k_z)},$$

where

$$[\|\mathbf{d}\|_2^2](k_x,k_z) := \int_0^{\infty}[\|\mathbf{d}\|_2^2](k_x,k_z,t)\,\mathrm{d}t := \int_0^{\infty}\int_{-1}^{1}\mathbf{d}^*(k_x,y,k_z,t)\mathbf{d}(k_x,y,k_z,t)\,\mathrm{d}y\,\mathrm{d}t.$$

On the other hand, the $\mathcal{H}_2$–norm has a stochastic interpretation: it quantifies the variance (energy) amplification of harmonic (in x and z) stochastic (in y and t) disturbances at any given pair (k_x,k_z) [11], [13]. This quantity is also referred to as the *ensemble average energy density* of the statistically steady-state [11]. Combining the definitions of the impulse response and the Hilbert–Schmidt norm, the $\mathcal{H}_2$–norm can be determined using either of the following two expressions

$$\begin{aligned}\left[\|\mathcal{H}\|_2^2\right](k_x,k_z) &= \mathrm{trace}\{\mathcal{C}(k_x,k_z)\mathcal{X}_\infty(k_x,k_z)\mathcal{C}^*(k_x,k_z)\} \\ &= \mathrm{trace}\{\mathcal{B}^*(k_x,k_z)\mathcal{Y}_\infty(k_x,k_z)\mathcal{B}(k_x,k_z)\},\end{aligned}$$

where, for stable systems, operators $\mathcal{X}_\infty(k_x,k_z)$ and $\mathcal{Y}_\infty(k_x,k_z)$ can be respectively obtained by solving the operator algebraic Lyapunov equations of the form

$$\begin{aligned}\mathcal{A}\mathcal{X}_\infty &+ \mathcal{X}_\infty\mathcal{A}^* &&= -\mathcal{B}\mathcal{B}^*, \\ \mathcal{A}^*\mathcal{Y}_\infty &+ \mathcal{Y}_\infty\mathcal{A} &&= -\mathcal{C}^*\mathcal{C}.\end{aligned}$$

The Hilbert-Schmidt norm of the impulse response operator can be also integrated over the finite time interval to yield:

$$\left[\|\mathcal{H}\|_2^2\right](k_x,k_z,t) := \int_0^t\|\mathcal{H}(k_x,k_z,\tau)\|_{HS}^2\,\mathrm{d}\tau.$$

The resulting measure of velocity perturbations can be determined as

$$\begin{aligned}\left[\|\mathcal{H}\|_2^2\right](k_x,k_z,t) &= \mathrm{trace}\{\mathcal{C}(k_x,k_z)\mathcal{X}_t(k_x,k_z)\mathcal{C}^*(k_x,k_z)\} \\ &= \mathrm{trace}\{\mathcal{B}^*(k_x,k_z)\mathcal{Y}_t(k_x,k_z)\mathcal{B}(k_x,k_z)\},\end{aligned}$$

where operators $\mathcal{X}_t(k_x,k_z)$ and $\mathcal{Y}_t(k_x,k_z)$ represent solutions of the following two differential Lyapunov equations

$$\begin{aligned}\frac{\mathrm{d}\mathcal{X}_t}{\mathrm{d}t} &= \mathcal{A}\mathcal{X}_t &+ \mathcal{X}_t\mathcal{A}^* &+ \mathcal{B}\mathcal{B}^*, \\ \frac{\mathrm{d}\mathcal{Y}_t}{\mathrm{d}t} &= \mathcal{A}^*\mathcal{Y}_t &+ \mathcal{Y}_t\mathcal{A} &+ \mathcal{C}^*\mathcal{C},\end{aligned} \tag{8}$$

with the initial conditions $\mathcal{X}_0(k_x,k_z)=0$ and $\mathcal{Y}_0(k_x,k_z)=0$, for every (k_x,k_z), respectively. For stable systems, these two operators can be determined based on [11]

$$\begin{aligned}\mathcal{X}_t &= \mathcal{X}_\infty - \mathrm{e}^{\mathcal{A}t}\mathcal{X}_\infty\mathrm{e}^{\mathcal{A}^*t}, \\ \mathcal{Y}_t &= \mathcal{Y}_\infty - \mathrm{e}^{\mathcal{A}^*t}\mathcal{Y}_\infty\mathrm{e}^{\mathcal{A}t}.\end{aligned} \tag{9}$$

It is well known that non-normal modes in the form of elongated streamwise structures dominate TS modes in subcritical channel flows. Among other tools, the analysis of the previously defined input-output system gains can be used to establish this [11]–[15]. It is a standard fact from control theory [18], [19] that both $\mathcal{H}_\infty$ and $\mathcal{H}_2$ norms are finite for stable causal dynamical systems. However, for flows occurring in supercritical regimes the quantities defined by (6) and (7) can become infinitely large. Because of that, we want to develop a computationally efficient procedure for studying the finite-horizon input-output gains for system (1) with unstable dynamics. In § III-A, we define these gains and argue that their analysis represents a non-trivial mathematical exercise. In § III-B, we show how these gains can be approximated by introducing the 'exponential discounting' in signals appearing in (1).

A. Finite horizon input-output gains

In this subsection we define the finite horizon input-output system gains for flows taking place in supercritical regimes. In particular, we want to analyze the induced finite horizon 2–norm. The definition of this norm in the temporal domain is given by

$$\left[\|\mathcal{H}_T\|_\infty\right](k_x,k_z) = \sup_{[\|\mathbf{d}_T\|_2](k_x,k_z)\,\leq\,1}\frac{[\|\phi_T\|_2](k_x,k_z)}{[\|\mathbf{d}_T\|_2](k_x,k_z)}, \tag{10}$$

where

$$[\|\mathbf{d}_T\|_2^2](k_x,k_z) := \int_0^T[\|\mathbf{d}\|_2^2](k_x,k_z,t)\,\mathrm{d}t := \int_0^T\int_{-1}^{1}\mathbf{d}^*(k_x,y,k_z,t)\mathbf{d}(k_x,y,k_z,t)\,\mathrm{d}y\,\mathrm{d}t.$$

Clearly, the measure of velocity perturbations defined by (10) represents a finite horizon equivalent of the previously defined $\mathcal{H}_\infty$–norm. This quantity assumes finite values even in supercritical flows, which is an appealing property. However, the computation of (10) is a non-trivial mathematical exercise (see, for example, [20]).

We can also study $\left[\|\mathcal{H}\|_2\right](k_x,k_z,t)$ in supercritical flows. It is noteworthy that for system (1) with unstable dynamics $\mathcal{X}_t$ and $\mathcal{Y}_t$ cannot be computed using (9) since both $\mathcal{X}_\infty$ and $\mathcal{Y}_\infty$ diverge in this case. Notwithstanding, $\left[\|\mathcal{H}\|_2\right](k_x,k_z,t)$ can be determined by performing the direct numerical integration of the finite dimensional equivalent of either of the two equations in (8). This would typically require solving a very large number of the Ordinary Differential Equations (ODEs) which is computationally inefficient. Because of that, in § III-B, we show how these finite horizon measures of velocity perturbations can be approximately determined by considering the 'exponentially discounted' versions of signals in (1).

B. Exponentially discounted input-output gains

In this subsection we consider supercritical channel flows and define the input-output gains for systems whose inputs and outputs represent 'exponentially discounted' versions of their LNS analogues, that is $\mathbf{d}_\alpha := \mathrm{e}^{-\alpha t}\mathbf{d}$, $\phi_\alpha := \mathrm{e}^{-\alpha t}\phi$,

with $\alpha > 0$. Transformation of this form renders the LNS equations into

$$\begin{aligned}\partial_t \psi_\alpha(k_x,y,k_z,t) &= [\mathcal{A}_\alpha(k_x,k_z)\psi_\alpha(k_x,k_z,t)](y) + \\ &\quad [\mathcal{B}(k_x,k_z)\mathbf{d}_\alpha(k_x,k_z,t)](y), \\ \phi_\alpha(k_x,y,k_z,t) &= [\mathcal{C}(k_x,k_z)\psi_\alpha(k_x,k_z,t)](y),\end{aligned} \tag{11}$$

where $\psi_\alpha := \mathrm{e}^{-\alpha t}\psi$ is the exponentially weighted state of the LNS equations. Input and output operators $\mathcal{B}$ and $\mathcal{C}$ have the same meaning as in (1), whereas the generator of (11) is obtained by shifting the generator of (1) by the amount proportional to the exponential discounting, i.e. $\mathcal{A}_\alpha(k_x,k_z) := \mathcal{A}(k_x,k_z) - \alpha I$. The frequency domain description of (11) is clearly given by $\phi_\alpha(k_x,y,k_z,\omega) = [\mathcal{H}_\alpha(k_x,k_z,\omega)\mathbf{d}_\alpha(k_x,k_z,\omega)](y) = [\mathcal{C}(k_x,k_z)((\mathrm{i}\omega+\alpha)I - \mathcal{A}(k_x,k_z))^{-1}\mathcal{B}(k_x,k_z)\mathbf{d}_\alpha(k_x,k_z,\omega)](y)$. If parameter α is chosen so that $\alpha > \sup_{k_x,k_z}\lambda_{\max}\{\mathcal{A}(k_x,k_z)\}$, than $\mathcal{A}_\alpha(k_x,k_z)$ represents an exponentially stable operator for any given pair of wave-numbers (k_x,k_z). Therefore, the net effect of exponential discounting in this case is stabilization of the LNS equations which implies that the $\mathcal{H}_\infty$ and $\mathcal{H}_2$–norms of system (11) can be computed using the procedure outlined in § III. In particular, the following interpretation can be given to the $\mathcal{H}_\infty$–norm of (11) in the time domain

$$[\|\mathcal{H}_\alpha\|_\infty](k_x,k_z) = \sup_{[\|\mathbf{d}_\alpha\|_2](k_x,k_z) \le 1} \frac{[\|\phi_\alpha\|_2](k_x,k_z)}{[\|\mathbf{d}_\alpha\|_2](k_x,k_z)},$$

where

$$\begin{aligned}&[\|\mathbf{d}_\alpha\|_2^2](k_x,k_z) := \\ &\int_0^\infty \int_{-1}^1 \mathbf{d}_\alpha^*(k_x,y,k_z,t)\mathbf{d}_\alpha(k_x,y,k_z,t)\,\mathrm{d}y\,\mathrm{d}t = \\ &\int_0^\infty \int_{-1}^1 \mathrm{e}^{-2\alpha t}\mathbf{d}^*(k_x,y,k_z,t)\mathbf{d}(k_x,y,k_z,t)\,\mathrm{d}y\,\mathrm{d}t = \\ &\int_0^\infty \mathrm{e}^{-2\alpha t}[\|\mathbf{d}\|_2^2](k_x,k_z,t)\,\mathrm{d}t.\end{aligned}$$

On the other hand, for a given pair (k_x,k_z) and $t > 0$, the 'finite horizon $\mathcal{H}_2$–norm' of system (1) at time t can be determined by the $\mathcal{H}_2$–norm of system (11), provided that the design parameter α is appropriately selected. This is because $[\|\mathcal{H}\|_2](k_x,k_z,t)$ represents a monotonically increasing function of time which is equal to zero at $t = 0$, and $[\|\mathcal{H}_\alpha\|_2](k_x,k_z)$ is a finite number for any given pair (k_x,k_z). Unfortunately, in general, it is very difficult to establish the exact correspondence between $[\|\mathcal{H}\|_2](k_x,k_z,t)$ and $[\|\mathcal{H}_\alpha\|_2](k_x,k_z)$. In other words, it is very hard to determine pair (t,α) at which $[\|\mathcal{H}\|_2](k_x,k_z,t) = [\|\mathcal{H}_\alpha\|_2](k_x,k_z)$. However, some intuition can be gained by considering the following scalar example

$$\left.\begin{aligned}\dot\psi &= a\psi + d \\ \phi &= \psi\end{aligned}\right\}, \quad a > 0, \tag{12}$$

with its 'exponentially discounted' equivalent of the form

$$\left.\begin{aligned}\dot\psi_\alpha &= (a-\alpha)\psi_\alpha + d_\alpha \\ \phi_\alpha &= \psi_\alpha\end{aligned}\right\}, \quad \alpha > a. \tag{13}$$

The 'finite horizon $\mathcal{H}_2$–norm' of system (12) and the $\mathcal{H}_2$–norm of system (13) are respectively given by

$$\begin{aligned}[\|H\|_2^2](t) &= \frac{1}{2a}(\mathrm{e}^{2at}-1), \\ \|H_\alpha\|_2^2 &= \frac{1}{2a(\alpha-a)},\end{aligned}$$

which implies that, for a chosen $\alpha > a$, $[\|H\|_2](t) = \|H_\alpha\|_2$ at

$$t = \frac{1}{2a}\ln\frac{\alpha}{\alpha-a}.$$

Equivalently, for a given $t > 0$, these two quantities are equal if α satisfies

$$\alpha = \frac{a\mathrm{e}^{2at}}{\mathrm{e}^{2at}-1}.$$

Therefore, both the location of the unstable pole and the desired time interval determine the value of parameter α for which the $\mathcal{H}_2$–norm of system (13) determines the 'finite horizon $\mathcal{H}_2$–norm' of system (12). Furthermore, the closer α to a and the smaller a, the larger time at which $[\|H\|_2](t) = \|H_\alpha\|_2$.

In § IV, we study the input-output gains in subcritical Poiseuille flow with $R = 5700$. We also compare the relative importance of non-normal and unstable modes in supercritical Poiseuille flow with $R = 10000$ by analyzing the exponentially discounted $\mathcal{H}_\infty$ and $\mathcal{H}_2$ system norms.

IV. Input-output gains in Poiseuille flow with $R = 5700$ and $R = 10000$

In this section, we study the input-output gains in subcritical Poiseuille flow with $R = 5700$, and the exponentially discounted input-output gains in supercritical Poiseuille flow with $R = 10000$ and $\alpha := 0.0038$. This particular choice of parameter α is made because the LNS equations have an unstable mode with a real part approximately equal to 0.0037 at $R = 10000$, $k_x = 1$, and $k_z = 0$ [21]. We compare the subcritical and supercritical results and show that they exhibit many qualitative similarities.

All results of this section are obtained numerically using the scheme described in [16], with 30 v and ω_y basis functions. The $\mathcal{H}_2$–norm–like quantities are determined based on solutions of the corresponding algebraic Lyapunov equations, with 50×90 grid points in the wave-number space (k_x,k_z). These points are chosen in the logarithmic scale with $\{k_{xmin} := 10^{-4}, k_{xmax} := 3.02\}$ and $\{k_{zmin} := 10^{-2}, k_{zmax} := 15.84\}$. On the other hand, the $\mathcal{H}_\infty$–norm–like quantities are calculated with $101 \times 90 \times 89$ grid points in the (k_x,k_z,ω) space. The frequency vectors in this case assume the forms: $\mathbf{k_x} := \begin{bmatrix} -\mathbf{k_{x1}} & 0 & \mathbf{k_{x1}} \end{bmatrix}$, $\mathbf{k_z} := \mathbf{k_{z1}}$, and $\boldsymbol{\omega} := \begin{bmatrix} -\omega_1 & 0 & \omega_1 \end{bmatrix}$, where $\mathbf{k_{x1}}$, $\mathbf{k_{z1}}$, and ω_1 are the vectors with 50, 90, and 44 logarithmically spaced points between $\{k_{xmin} := 10^{-4}, k_{xmax} := 3.02\}$, $\{k_{zmin} := 10^{-2}, k_{zmax} := 15.85\}$, and $\{\omega_{min} := 10^{-3}, \omega_{max} := 2\}$, respectively. All plots are given in the log–log–log scale.

A. Input-output gains in Poiseuille flow with $R = 5700$

Figure 2 shows the $\mathcal{H}_\infty$ and $\mathcal{H}_2$–norms of the operator $\mathcal{H}$ as functions of k_x and k_z, in subcritical Poiseuille flow with $R = 5700$. Despite the fact that the equations are about to become unstable if the Reynolds number is slightly increased (critical value of Reynolds number is approximately equal to 5772, [21]), the least-stable modes of generator $\mathcal{A}$ are not most amplified by system's dynamics. Rather, the largest input-output gains are attained for small streamwise wave-numbers at certain non-zero $O(1)$ value of k_z. This implies that the most amplified structures have very large streamwise elongation and spanwise periodicity determined by the value of k_z at which maximum happens to be. We remark that the peaks corresponding to the least-stable modes have much bigger values here than, for example, at $R = 2000$ [14], [15]. These peaks would go to infinity if the Reynolds number is increased above its critical value. However, this is an artifact of the

definition of the $\mathcal{H}_\infty$ and $\mathcal{H}_2$–norms rather than something that would play a dominant role in the initial stages of laminar-turbulent transition in flows that have some amount of background disturbances in them. This is further illustrated in the next subsection where we analyze the exponentially discounted input-output gains in supercritical Poiseuille flow with $R = 10000$.

B. Exponentially discounted input-output gains in Poiseuille flow with $R = 10000$

The left plot in Figure 3 illustrates the dependence of the exponentially discounted $\mathcal{H}_\infty$–norm on both streamwise and spanwise wave-numbers. The global maximum of the input-output gain visualized in this way occurs at $k_x = 0$ for certain non-zero $O(1)$ spanwise wave-number. It is important to remark that these dominant input-output resonances do not correspond to the exponentially growing modes of the generator $\mathcal{A}$. Rather, they are a product of the coupling from the wall-normal velocity to the wall-normal vorticity, which depends upon shear U' and spanwise frequency k_z [13]. This coupling is physically generated by the vortex tilting mechanism [22], [23]. Numerical experiments of [24] showed that without the coupling from v to ω_y the near-wall turbulence decays in a fully turbulent channel flow. The two-dimensional unstable modes of the operator $\mathcal{A}$ create a local peak at $k_z = 0$ and $k_x \approx 1$. The corresponding amplification is significantly lower than the one achieved by dominant streamwise constant flow structures. We also notice local three-dimensional peaks occurring at $k_x \approx 0.85$ and $k_z \approx 0.38$. These peaks are caused by the three-dimensional TS waves and they clearly induce larger input-output gains than the two dimensional exponentially growing normal modes. This further illustrates the importance of the three dimensional analysis which has traditionally been neglected owing to the misinterpretation of the Squire theorem (for more detail see, for example, [1] and discussions therein).

The exponentially discounted $\mathcal{H}_2$–norm is shown in the right plot of Figure 3. As for $[\|\mathcal{H}_\alpha\|_\infty](k_x, k_z)$, the global maximum takes place at $(k_x = 0, k_z = O(1))$. The peaks arising due to the exponentially growing eigenvalues of $\mathcal{A}$ are not as pronounced as their equivalents in $[\|\mathcal{H}_\alpha\|_\infty](k_x, k_z)$, due to the integration in time. Thus, the analysis of the variance accumulated on finite horizons indicates that in stochastically excited supercritical channel flows the most amplified input-output resonances (over long, but finite times) assume the form of streamwise vortices and streaks.

The results of this section illustrate that even a small amount of external excitation in supercritical flows yields completely different flow patterns from the ones corresponding to the exponentially growing system modes when finite time phenomena are considered. In particular, our results underscore the importance of the streamwise elongated flow structures not only in the subcritical channel flows, but also in the channel flows occurring in the supercritical regimes. We have also demonstrated the striking similarity between the supercritical and subcritical flows when the former are analyzed using the exponentially discounted system gains. The fact that the frequency response peaks produced by the TS waves (especially the three dimensional ones) achieve much higher magnitudes than the corresponding peaks in subcritical channel flows at moderate Reynolds numbers (e.g. $R = 2000$) suggests that most turbulent flows probably have both instabilities and high amplification of background disturbances.

V. Concluding remarks

This paper illustrates the significance of non-modal effects in supercritical channel flows. This is done by analyzing the LNS equations from an input-output point of view in the presence of 'exponentially discounted' input and output signals. From a physical perspective this type of analysis amounts to accounting for the finite time phenomena rather than the asymptotic phenomena of infinite time limits. In particular, our results underscore the importance of the streamwise elongated flow structures (that is, streamwise vortices and streaks) not only in the subcritical channel flows, but also in the channel flows taking place in the supercritical regimes.

It is quite compelling to argue that long-but-finite time analysis is relevant when considering linearized models. These models are not expected to be valid for infinite time in any case, as when perturbations grow, the linearized dynamics are altered. In the supercritical channel flow case, we see that the main features of the model (i.e., the modes contributing the most to perturbation energy) are very dependent on whether we take an infinite time limit or a large-but-finite time limit. The latter is arguably the more reasonable of the two, and when viewed this way, we have shown that aside from the energy of the perturbation, the spectral content of subcritical and supercritical channel flows is qualitatively very similar.

References

[1] P. J. Schmid and D. S. Henningson, *Stability and Transition in Shear Flows*. New York: Springer-Verlag, 2001.

[2] P. G. Drazin and W. H. Reid, *Hydrodynamic Stability*. Cambridge University Press, 1981.

[3] L. N. Trefethen, A. E. Trefethen, S. C. Reddy, and T. A. Driscoll, "Hydrodynamic stability without eigenvalues," *Science*, vol. 261, pp. 578–584, 1993.

[4] P. J. Schmid, S. C. Reddy, and D. S. Henningson, "Transition thresholds in boundary layer and channel flows," in *Advances in Turbulence VI*, S. Gavrilakis, L. Machiels, and P. A. Monkewitz, Eds. Kluwer, 1996.

[5] S. C. Reddy, P. J. Schmid, J. S. Baggett, and D. S. Henningson, "On stability of streamwise streaks and transition tresholds in plane channel flows," *J. Fluid Mech.*, vol. 365, pp. 269–303, 1998.

[6] S. J. Chapman, "Subcritical transition in channel flows," *J. Fluid Mech.*, vol. 451, pp. 35–97, 2002.

[7] A. Bottaro, P. Corbett, and P. Luchini, "The effect of base flow variation on flow stability," *J. Fluid Mech.*, vol. 476, pp. 293–302, 2003.

[8] L. H. Gustavsson, "Energy growth of three-dimensional disturbances in plane Poiseuille flow," *J. Fluid Mech.*, vol. 98, p. 149, 1991.

[9] K. M. Butler and B. F. Farrell, "Three-dimensional optimal perturbations in viscous shear flow," *Physics of Fluids A*, vol. 4, p. 1637, 1992.

[10] S. C. Reddy and D. S. Henningson, "Energy growth in viscous channel flows," *J. Fluid Mech.*, vol. 252, pp. 209–238, 1993.

[11] B. F. Farrell and P. J. Ioannou, "Stochastic forcing of the linearized Navier-Stokes equations," *Physics of Fluids A*, vol. 5, no. 11, pp. 2600–2609, 1993.

[12] ——, "Variance maintained by stochastic forcing of non-normal dynamical systems associated with linearly stable flows," *Physical Review Letters*, vol. 72, no. 8, pp. 1188–1191, 1994.

[13] B. Bamieh and M. Dahleh, "Energy amplification in channel flows with stochastic excitation," *Physics of Fluids*, vol. 13, no. 11, pp. 3258–3269, 2001.

[14] M. R. Jovanović and B. Bamieh, "Componentwise energy amplification in channel flows," *submitted to J. Fluid Mech.*, 2003, available at http://www.me.ucsb.edu/~jmihailo/publications/jfm03.html.

[15] ——, "Frequency domain analysis of the linearized Navier-Stokes equations," in *Proceedings of the 2003 American Control Conference*, Denver, CO, 2003, pp. 3190–3195.

[16] ——, "The spatio-temporal impulse response of the linearized Navier-Stokes equations," in *Proceedings of the 2001 American Control Conference*, Arlington, VA, 2001, pp. 1948–1953.

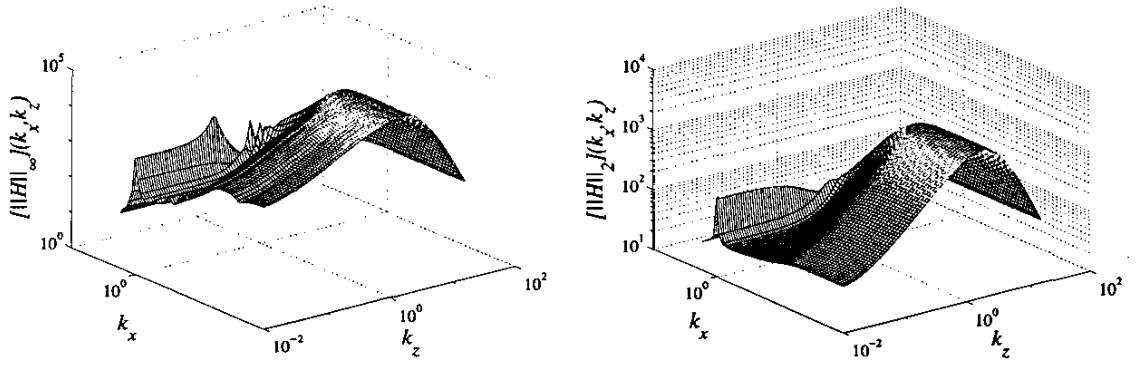

Fig. 2. Plots of $[\|\mathcal{H}\|_\infty](k_x, k_z)$ and $[\|\mathcal{H}\|_2](k_x, k_z)$ in Poiseuille flow with $R = 5700$.

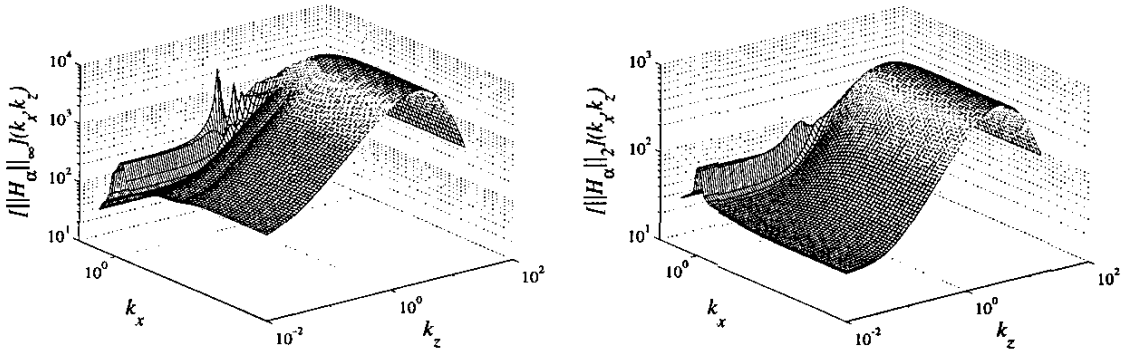

Fig. 3. Plots of $[\|\mathcal{H}_\alpha\|_\infty](k_x, k_z)$ and $[\|\mathcal{H}_\alpha\|_2](k_x, k_z)$ in Poiseuille flow with $R = 10000$ and $\alpha = 0.0038$.

[17] R. F. Curtain and H. J. Zwart, *An Introduction to Infinite-Dimensional Linear Systems Theory*. New York: Springer-Verlag, 1995.

[18] K. Zhou, J. C. Doyle, and K. Glover, *Robust and Optimal Control*. Prentice Hall, 1996.

[19] G. E. Dullerud and F. Paganini, *A course in robust control theory: a convex approach*. New York: Springer-Verlag, 2000.

[20] G. E. Dullerud, "Computing the L_2-induced norm of a compression operator," *Systems and Control Letters*, vol. 37, pp. 87–91, 1999.

[21] S. A. Orszag, "Accurate solution of the Orr-Sommerfeld equation," *J. Fluid Mech.*, vol. 50, pp. 689–703, 1971.

[22] M. T. Landahl, "Wave breakdown and turbulence," *SIAM J. Appl. Math.*, vol. 28, pp. 735–756, 1975.

[23] ——, "A note on an algebraic instability of inviscid parallel shear flows," *J. Fluid Mech.*, vol. 98, pp. 243–251, 1980.

[24] J. Kim and J. Lim, "A linear process in wall-bounded turbulent shear flows," *Physics of Fluids*, vol. 12, no. 8, pp. 1885–1888, 2000.